Delft University of Technology

In-Situ Characterization of Isotropic and Transversely Isotropic Elastic Properties Using Ultrasonic Wave Velocities

Pant, S; Laliberte, J; Martinez, Marcias; Rocha, B.

Important note
To cite this publication, please use the final published version (if applicable).
Please check the document version above.

In-situ characterization of isotropic and transversely isotropic elastic properties using ultrasonic wave velocities

S. Pant[1], J. Laliberte[1], M. Martinez[2,3], B. Rocha[4]

[1] Department of Mechanical and Aerospace Engineering, Carleton University,
3135 Mackenzie, 1125 Colonel By Drive, Ottawa, Ontario, K1S-5B6, Canada.

[2] Department of Mechanical and Aeronautical Engineering, Clarkson University,
8 Clarkson Avenue, Potsdam, NY 13699-5725 USA

[3] Faculty of Aerospace Engineering, Delft University of Technology,
Building 62, Kluyverweg 1, 2629 HS Delft, P.O. Box 5058, 2600 GB Delft, The Netherlands

[4] Department of Mechanical and Transportation Technology, Algonquin College,
1385 Woodroffe Ave, Ottawa, Ontario, K2G-1V8, Canada.

Corresponding Author (shashankpant@cmail.carleton.ca)

Abstract

In this paper a one-sided, *in-situ* method based on the time of flight measurement of ultrasonic waves is described. The primary application of this technique is to non-destructively measure the stiffness properties of isotropic and transversely isotropic materials. The method consists of generating and receiving quasi-longitudinal and quasi-shear waves at different through-thickness propagation angles. First, the analytical equations are provided to calculate the ultrasonic wave velocities. Then, an inverse method based on non-linear least square technique is used to calculate the stiffness constants using the ultrasonic wave velocities. Sensitivity analysis is performed by randomly perturbing the velocity data, thus observing the effects of perturbations on the calculated stiffness constants. An improved algorithm is proposed and tested to reduce the effects of random errors. Based on the sensitivity analysis, minimum number of angles required to inversely calculate the stiffness constants are suggested for isotropic and transversely isotropic material. The method was experimentally verified on an isotropic 7050-T7451 aluminum with two different thicknesses and a transversely isotropic composite laminate fabricated using 24 plies of CYCOM 977-2 12 k HTA unidirectional carbon fibre reinforced polymer (CFRP) prepregs. The results demonstrate that this technique is able to accurately measure the material properties of isotropic material. As for the transversely isotropic material this method is able to accurately measure the material properties if the experimental errors can be reduced to less than 1%.

Keywords

Material characterization, ultrasound wave velocities, composite, non-destructive evaluation, material stiffness constants

1 Introduction

Material elastic properties such as tensile stiffness, shear stiffness, and Poisson's ratio are required by engineers for analyzing stress-strain response, vibration behaviour, stress wave propagation, and for finite element analysis. The most widely used experimental techniques for determining such properties are by conducting tension, shear, bending, and torsion tests following ASTM and ISO standards. The standard tests require small, discrete samples of the same structural materials to be evaluated and are for the most part destructive in nature. Sometimes the samples may not be available for an already manufactured structure or ageing of the structure may have caused the material properties to change. As such, the

experimental results from the discrete samples may not be truly representative of the final or in service component. To overcome this problem, non-destructive methods such as ultrasonic waves using time of flight analysis and Lamb waves have been used to find the elastic properties of the material. Typically these properties consist of: Poisson's ratio, tensile and shear stiffness in different directions for isotropic and anisotropic medium [1]. This paper focuses on the use of ultrasonic waves' time of flight for material property determination.

The most commonly used ultrasonic methods for determining the stiffness constants for an isotropic solid consist on directly measuring the pure longitudinal and shear velocities across the thickness using pulse-echo [2] or through-transmission technique [3]. The stiffness constants E, G, and Poisson's Ratio (μ) are directly related to these velocities [4]. In the case of transversely isotropic media, the stiffness constants are calculated using the ultrasonic phase/group velocities, which require: (i) cutting the specimen in a predetermined crystallographic plane or (ii) by using an immersion technique. In the cutting technique, the samples are cut along a predetermined direction and the velocities are measured along those directions to directly calculate the stiffness constants [5]. In the immersion techniques, the sample is immersed in a liquid where quasi-longitudinal and quasi-shear waves are generated at oblique angles to the liquid-solid interface [6]. Poisson's ratio has also been calculated by combining ultrasonic and mechanical tests, where Young's modulii and normal stiffness tensor were measured using mechanical tests and through-transmission ultrasonic tests respectively [7]. One drawback of the aforementioned methods is that small samples from the material or structure being analyzed where access to both sides may be required. This may not be feasible for in-service components or components where access to only one side is available.

In this paper an *in-situ* method based on the through-thickness propagation of ultrasonic wave is presented and experimentally verified for isotropic and transversely isotropic material. The method consists of generating and receiving quasi-longitudinal (QL) and quasi-transverse (QT) waves at different through-thickness propagation angles requiring access to only one side of the specimen. An inverse algorithm based on non-linear least square technique is developed to calculate the material constants from the QL and QT wave velocities.

2 Materials and Methods

Two different thicknesses of isotropic 7050-T7451 aluminum and one transversely isotropic carbon-fiber/epoxy laminate constructed with 24 plies of CYCOM 977-2 12k HTA unidirectional prepregs were tested. The experimental schematic and test setup is shown in Figure 1.
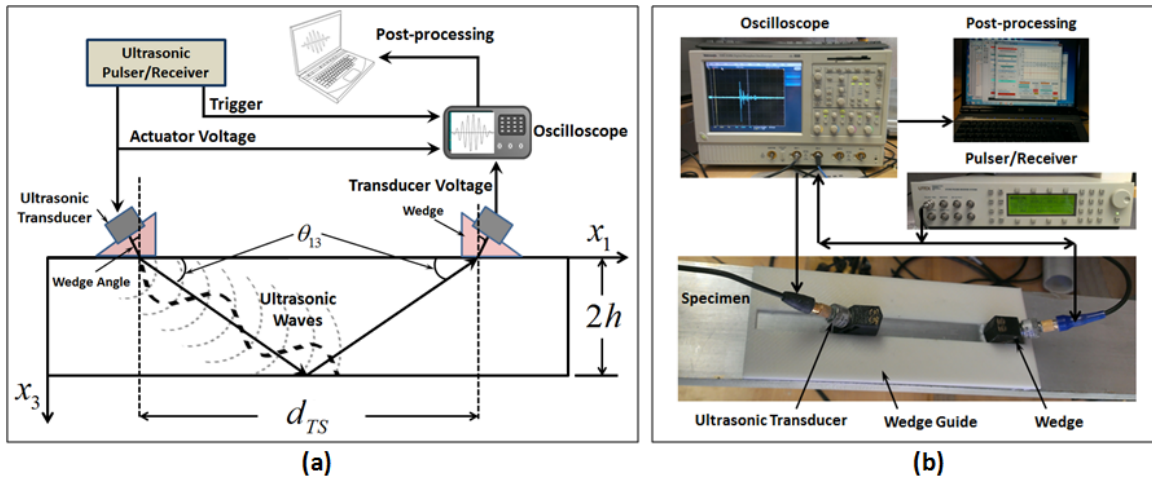
Figure 1: Experimental (a) schematic and (b) setup to generate and gather ultrasonic waves

Referring to Figure 1, *UTEX UT340* pulser/receiver system was used to send a short-pulse of 100V amplitude signal to a broadband *Panametrix 5MHz/0.25"/C543-SM* ultrasonic transducers as well as a trigger signal to start the *Tektronix TDS 5104* digital oscilloscope. The ultrasonic waves generated by the pulse signal propagate through the sample thickness at an angle θ_{13} (Figure 1a) and are reflected from the back surface; a second ultrasonic transducer of the same type picks up the reflected wave signal. The distance d_{TS} (Figure 1a) between the actuating and sensing transducers was varied in a straight line with the help of a wedge guide to find the maximum signal strength received by the sensing transducer. Once the maximum signal strength was received, data were acquired at a rate of 125 MS/s and exported to Matlab as a (.mat) file for post-processing. Software was developed in Matlab to process the data and to extract the ultrasonic wave velocity. Custom made angled-wedges were used to generate the QL and QT waves at different angles for isotropic and transversely isotropic specimen. Different angled-wedges were needed to excite the QL and QT waves following the Snell's Law. As shown in Figure 2, below the first critical angle (angle above which no energy is propagated into the solid) both QL and QT waves are present. Whereas, between the first and the second critical angles only QT waves are present at lower wedge angles, while QT and Surface Waves (SW) are present at higher wedge angles. Above the second critical angle only SW are present [8]. The wedges were designed and then printed in a Stratasys Dimension 3D printer, with the holes filled with *Westsystem 105 Epoxy resin* with *205 Fast-hardener*.
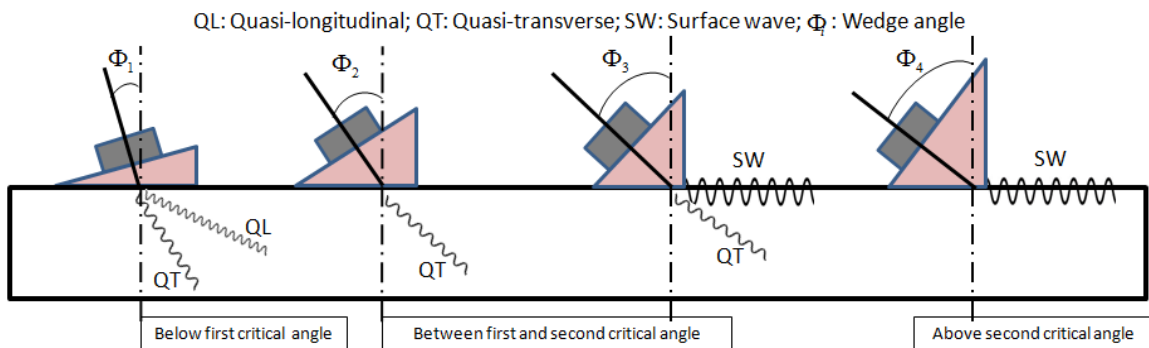
Figure 2: Modes of ultrasonic wave propagations at various wedge angles

Acquired signals were calibrated to incorporate the time taken for the ultrasound to travel through the wedge and into the sample. This was done by measuring the time for the ultrasound to travel from the

actuating transducer to the sensing transducer for all sets of angled-wedges. It was also found that there was a delay between the pulse generated by the pulser/receiver and the ultrasound generated by the transducer. This was due to the time-delay or rise-time for the piezoelectric element used in the transducer to react to the applied short pulse high voltage signal. The time of travel was found by tracking the peak of the initial pulse and the wave signal received by the receiving transducer. The total time delay was added to the acquired initial pulse when calculating the QL and QT wave velocities. The stiffness constants were calculated using the experimentally determined QL and QT wave velocities at different through-thickness propagation angles θ_{13} (Figure 1a) excited using different angled-wedges.

2.1   Numerical Solution and Optimization

There are several methods to inversely calculate and optimize the stiffness constants for isotropic and transversely isotropic material using the measured phase/group velocities. Some of the most commonly used methods include: genetic algorithms (GA) [9], non-linear least square method [10], or a combination of both [11]. Before using the experimental data to determine the stiffness constant, it is necessary to verify the optimization algorithm. These optimization algorithms can be sensitive to the experimental errors associated with the measurement of the QL and QT wave velocities. For this purpose, a non-linear least square method was first used to find the stiffness constants of a known isotropic and transversely isotropic material. Refer to Appendix A for the derivation and explanation of equations used for calculating the material stiffness.

For the isotropic material, the theoretically calculated phase velocities along $\left(x_1 - x_3\right)$ plane with varying through-thickness propagation angles θ_{13} (Figure A1) were used. The functions to be minimized are given by Eqn. (A.7) to determine the stiffness constants $\left(c_{11}, c_{13}, c_{33}, c_{55}\right)$ by minimizing the error between the calculated and experimental phase velocities of QL and QT waves as shown in the equation below:

$$\min \sum_{i=1}^{n} \left[\left(V_{p_{Calculated}}\right)_i - \left(V_{p_{Measured}}\right)_i\right]^2 \tag{2.1}$$

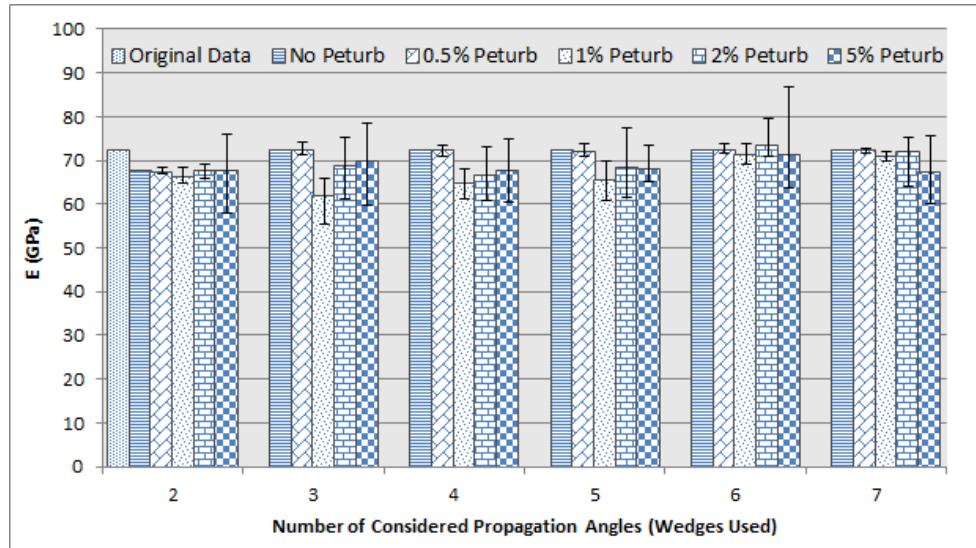Where, n is the number of different propagation angles and V_p is the phase velocity.

2.1.1   Sensitivity Analysis for Isotropic Material

The non-linear least square algorithm was first analytically verified on an isotropic (Al 2024-T6) with the known properties of elastic stiffness (E) = 72.4 GPa, shear stiffness (G) = 27.2GPa, and Poisson's Ratio $\left(\mu\right)$= 0.33 [12]. The phase velocities were calculated analytically using Eqn. (A.7) by considering the QL and QT waves propagating at $\theta_{12} = 0^o$ along θ_{13} at [60/65/70/75/80/85/90] and [25/30/35/40/45/50/55] degrees respectively (Figure A1). Higher angles of θ_{13} were considered for QL as compared to QT due to Snell's Law of Refraction. The flow chart of the method initially used to find the material constants $\left(E, G, \mu\right)$ of an isotropic solid is shown in Figure 3.
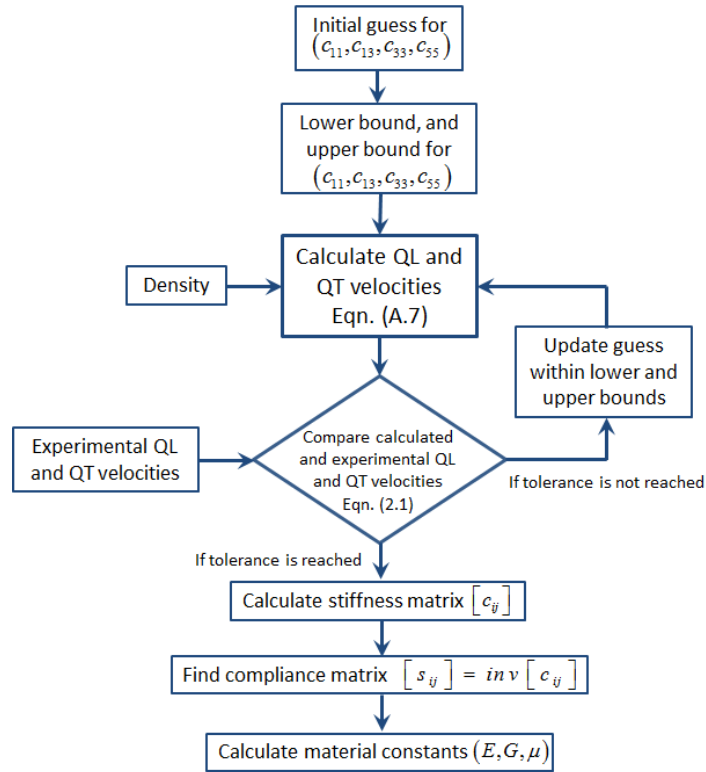
Figure 3: Initially used non-linear least square method to calculate material constants

The QL and QT wave velocities at a given sets of propagation angle were randomly perturbed by 0.5, 1, 2, and 5 percent from their original values ten times to get ten data points (ten QL and ten QT velocities) for inversely calculating the stiffness constants. This study was performed in order to find out how the number of experimental readings, the number of propagation angles considered (number of different angled-wedges needed to generate the waves), and the effect of random variation in the experimental data influences the convergence of calculated material stiffness constants. The results, as shown in Figure 4 to Figure 6 for E, G, and Poisson's Ratio can be used to select the minimum number of propagation angles. Thus, the number of different angled-wedges needed to generate the QL and QT waves for an isotropic solid to inversely calculate the stiffness constants.
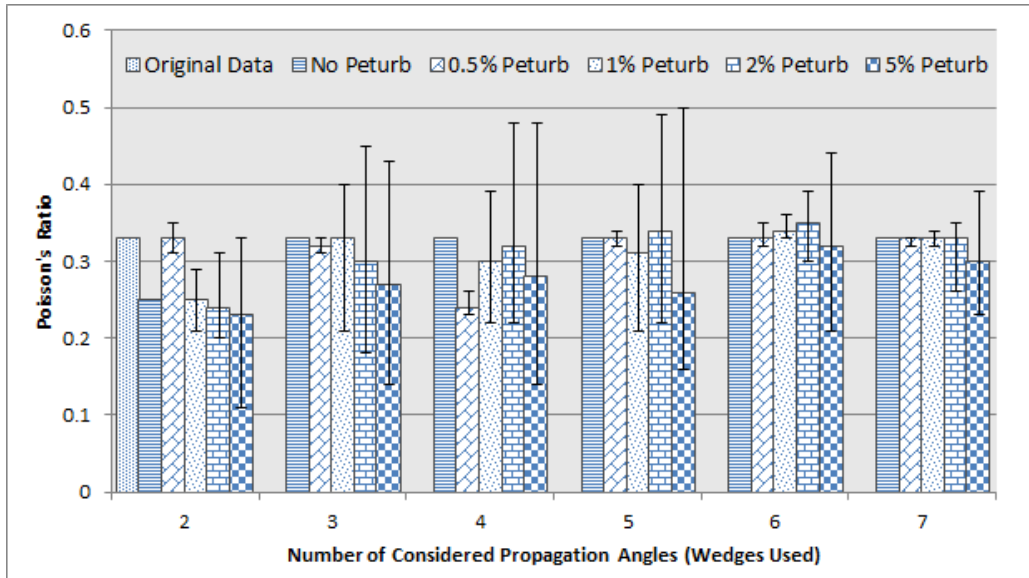
Figure 4: Initial convergence summary of elastic stiffness (*E*)

Figure 4 shows the convergence of the elastic stiffness as groups of bar graphs plotted against the number of propagation angles considered (2 to 7), where different percent perturbations are shown in cross-hatches increasing from left to right. The grouped bar graphs represent the average values of ten runs, where the minimum and maximum values are shown by the error bars.
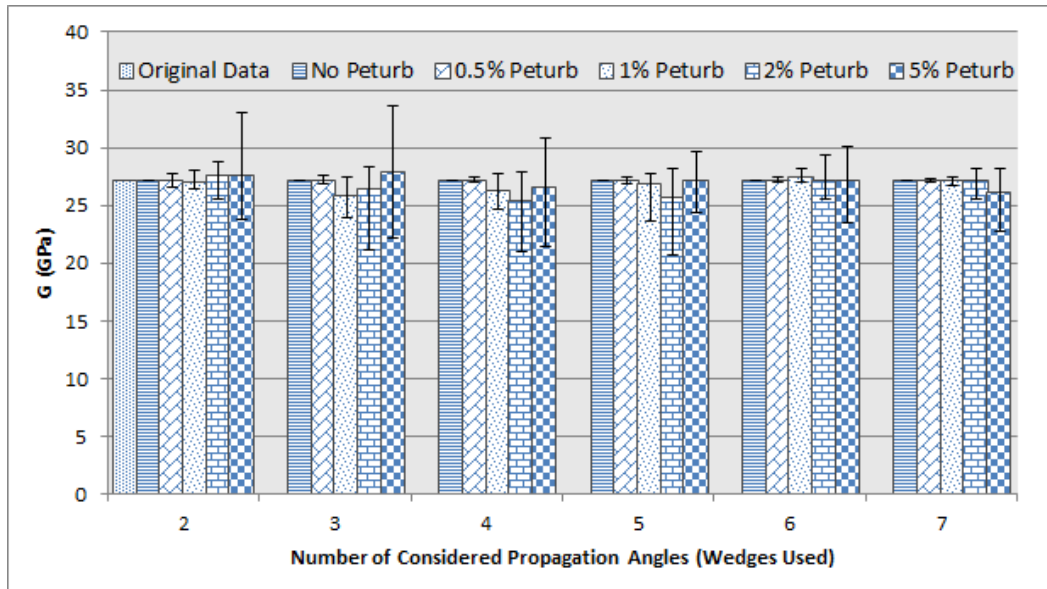

Figure 5: Initial convergence summary of shear stiffness (*G*)

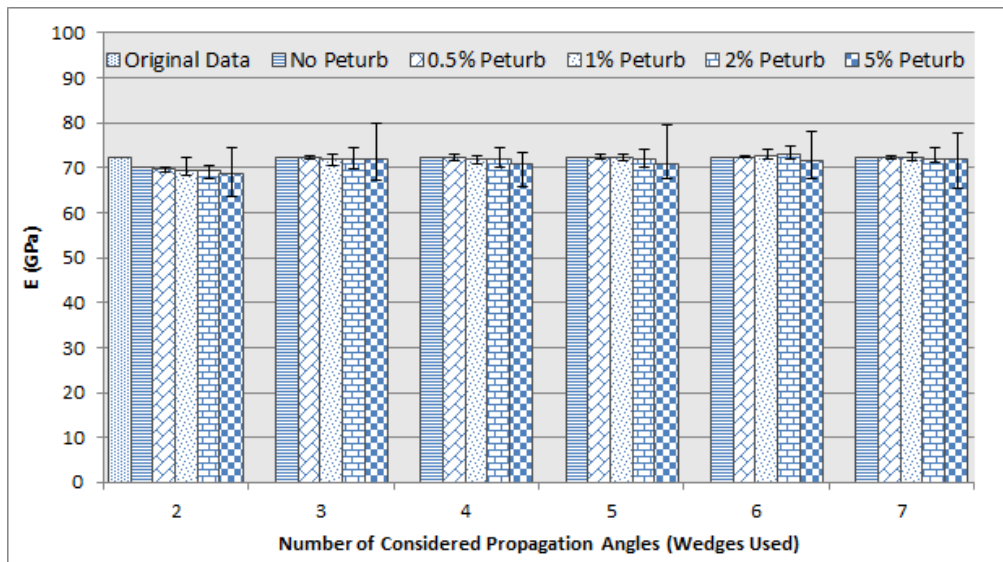**Figure 6: Initial convergence summary of Poisson's ratio (μ)**

From Figure 4 to Figure 6 above, it can be seen that six different propagation angles are needed for convergence due to random perturbation errors of approximately 1%. Even without perturbation, the algorithm did not converge if only two sets of propagation angles were considered. This indicated the need for at least three different sets of angles for the experiments (three for QL and three for QT). As can be seen from Figure 4 and Figure 6, the errors associated with the data scatter of E and Poisson's ratio respectively were higher when compared to G shown in Figure 5. Therefore, an improvement in the least-squared algorithm for an isotropic material presented above was performed by comparing the stiffness matrix constants c_{11} and c_{33}. Knowing that c_{11} should equal to c_{33} for an isotropic material, a bisection method was implemented to minimize the difference between c_{11} and c_{33}. This was performed by letting the other two variable (c_{13}, c_{55}) change between the upper and lower bounds in order to satisfy the imposed equality condition. The improved optimization method is shown in Figure 7 within the dotted box.
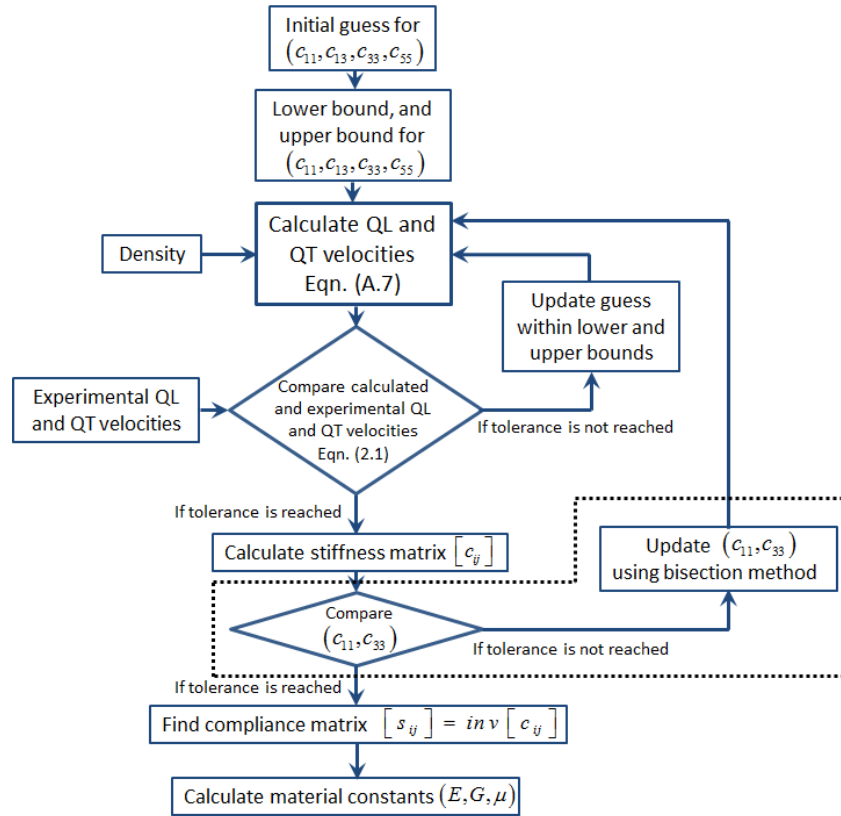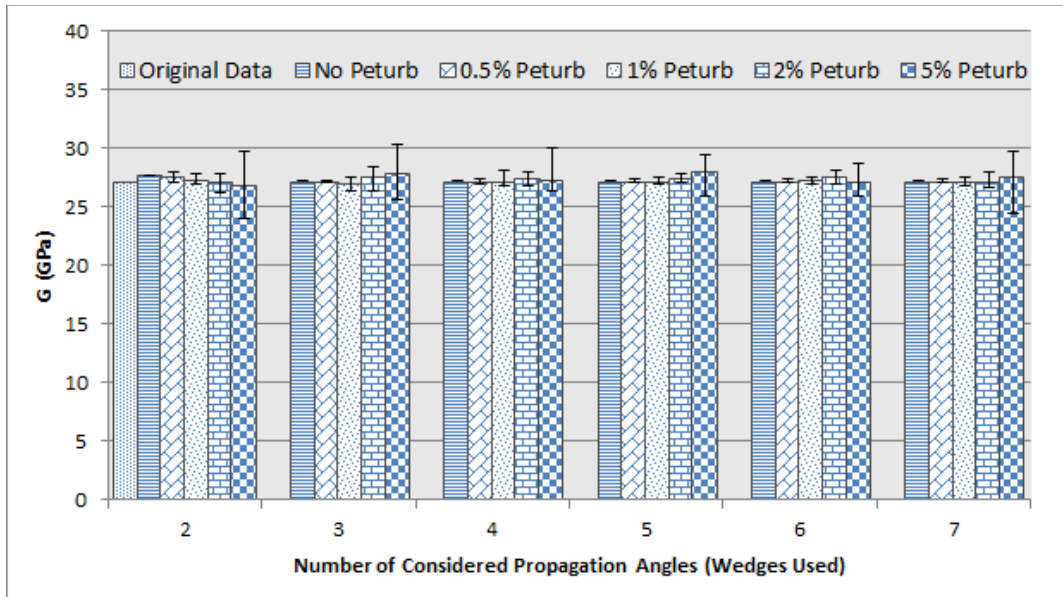
**Figure 7: An improved method to calculate material stiffness constants**

The convergence summary and the data scatter plot after implementing the bisection method on the same sets of data used previously are shown in Figure 8 to Figure 10.

Figure 8: Convergence summary of elastic stiffness (E) using improved algorithm

Figure 9: Convergence summary of shear stiffness (*G*) using improved algorithm
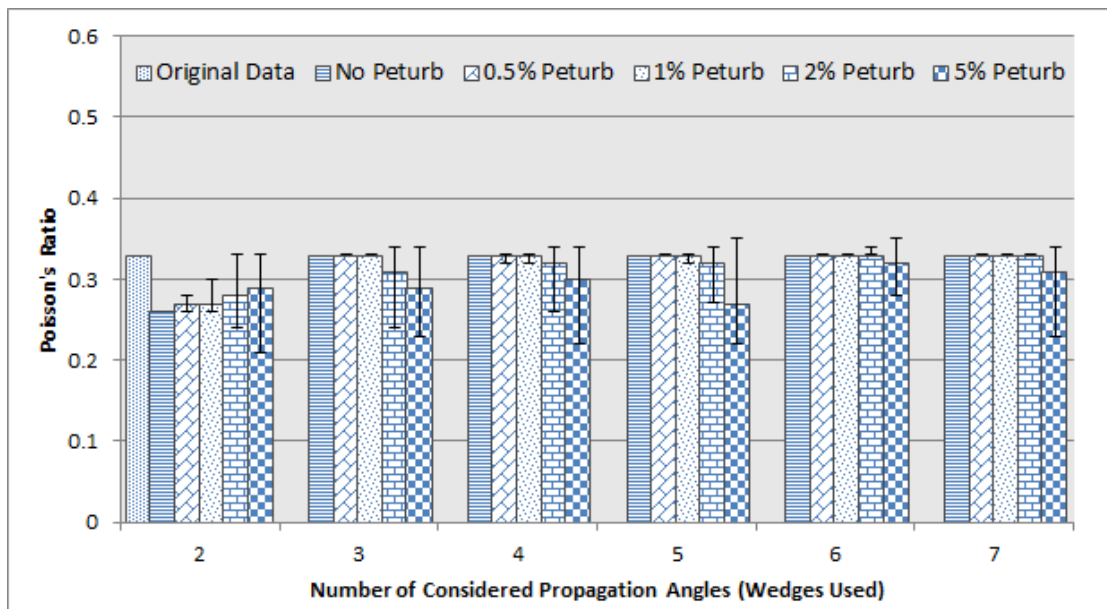
Figure 10: Convergence summary of Poisson's ratio (*μ*) using improved algorithm

By comparing Figures 4 to 6 with Figures 8 to 10, it can be seen that implementing the bisection search greatly improved the convergence results and minimized the spread (difference between maximum and minimum value). The improved algorithm also reduced the number of required propagation angles from six to three in order to counteract up to 1% of random errors found by comparing the original data to the average calculated values. For example, in Figure 10, the bar graph of 3 propagation angles at 1% perturbation is equal to the original data, whereas at 2%, the value is lower than the original data. It can be seen that the refined algorithm still did not converge if only two sets of propagation angles were considered. Hence a minimum of three propagation angles are required for both QL and QL waves. Results were similar when the algorithm was tested on an isotropic Ti-6Al-4V alloy. It was also found

that changing the initial guesses and the upper bounds had no effect on the final results, further proving the robustness of the improved algorithm.

## 2.1.2 Sensitivity Analysis for Transversely Isotropic Material

The algorithm for a transversely isotropic material was verified on a previously researched composite laminate (Cytec G40-800/5276-1) with known stiffness properties provided in Table 1 [13]. The QL and QT phase velocities were calculated analytically using Eqn. (A.7) and Eqn. (A.8) provided in Appendix A for $\theta_{12} = 0^\circ$ and $\theta_{12} = 90^\circ$ (Figure A1) respectively.

Table 1: Material properties for Cytec G40-800/5276-1 laminate

E_{11}	E_{22}	G_{12}	μ_{12}	μ_{23}	Density
143 GPa	9.1 GPa	4.8 GPa	0.3	0.3	1650 kg/m^3

Similar to the isotropic case, the propagation angles for θ_{13} and θ_{23} (Figure A1) were chosen at [65/70/ 75/80/85/90] and [30/35/40/45/50/55] degrees to generate QL and QT waves respectively. Figure 11 shows the flow chart of the method initially used to calculate the stiffness constants.

Referring to Figure 11; first, the initial guesses along with the lower/upper bounds for the stiffness constants $(c_{11}, c_{13}, c_{33}, c_{55})$ and $(c_{22}, c_{23}, c_{33}, c_{44})$ were chosen. Then, Eqn. (A.7) and Eqn. (A.8) were used to calculate the QL and QT wave velocities using the initial guesses for $(c_{11}, c_{13}, c_{33}, c_{55})$ and $(c_{22}, c_{23}, c_{33}, c_{44})$ respectively. The calculated and the experimentally measured QL and QT wave velocities were compared for wave propagating in the $(x_1 - x_3)$ and $(x_2 - x_3)$ plane using left hand side and right hand side (RHS) of the algorithm respectively. The guesses for $(c_{11}, c_{13}, c_{33}, c_{55})$ and $(c_{22}, c_{23}, c_{33}, c_{44})$ were updated within the lower and upper bounds to calculate and compare the analytical and experimental wave velocities. This process was repeated until the desired tolerance was reached. Then, the stiffness constants were assembled into a 6x6 stiffness matrix $\left[c_{ij} \right]$, which was inverted to find the compliance matrix $\left[s_{ij} \right]$. Using the terms in the 6x6 compliance matrix, the material constants (E_{11}, E_{22}, G_{12}, μ_{12}, and μ_{23}) were calculated.
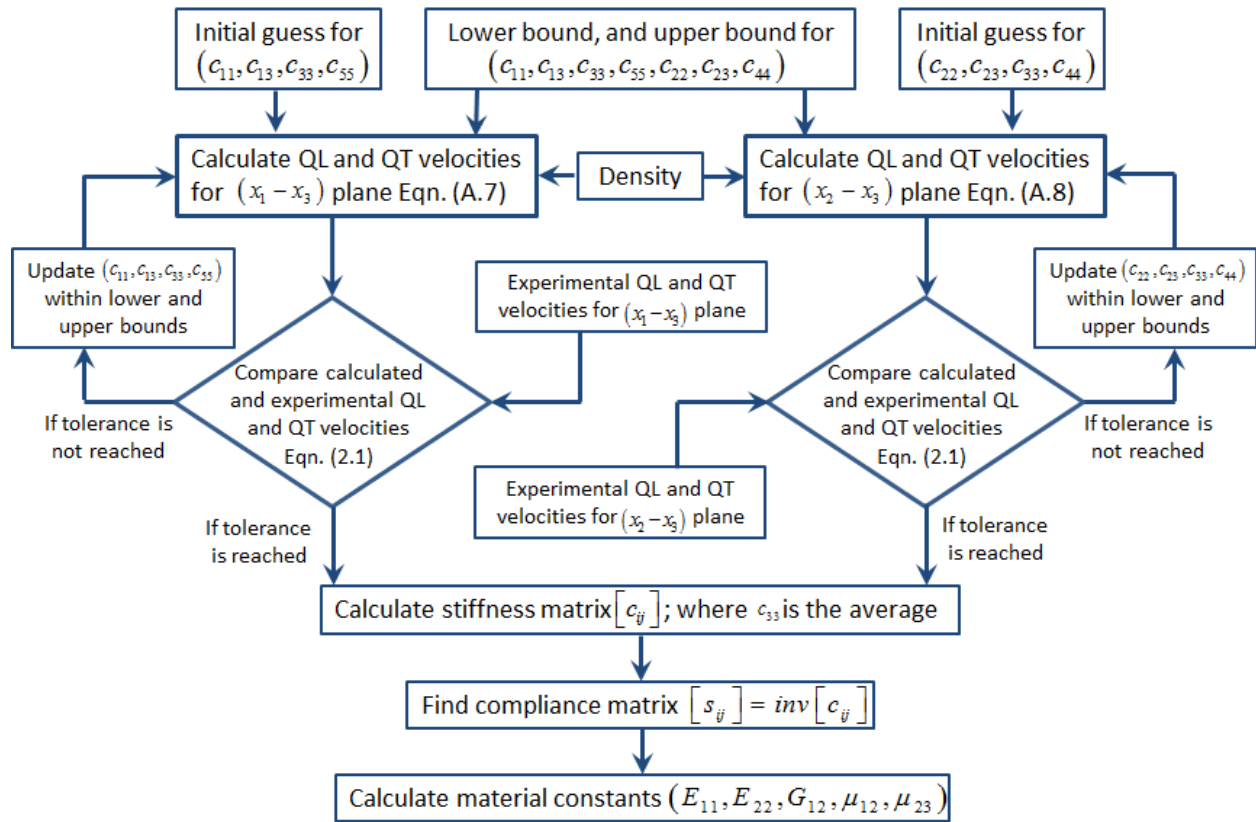
Figure 11: Flow chart to calculate stiffness constants of a transversely isotropic material

Similar to the isotropic case, the QL and QT wave velocities were randomly perturbed by 0.5, 1, 2, and 5 percent from their original values ten times. However, during these perturbations, the propagation angles were kept constant as to generate a total of ten data points for each perturbation. The results shown in Figure 12 to Figure 16 for E_{11}, E_{22}, G_{12}, and Poisson's ratios (μ_{12}, μ_{23}) respectively can be used to select the minimum number of propagation angles needed to generate the QL and QT waves for inversely calculating the stiffness constants of a transversely isotropic material.
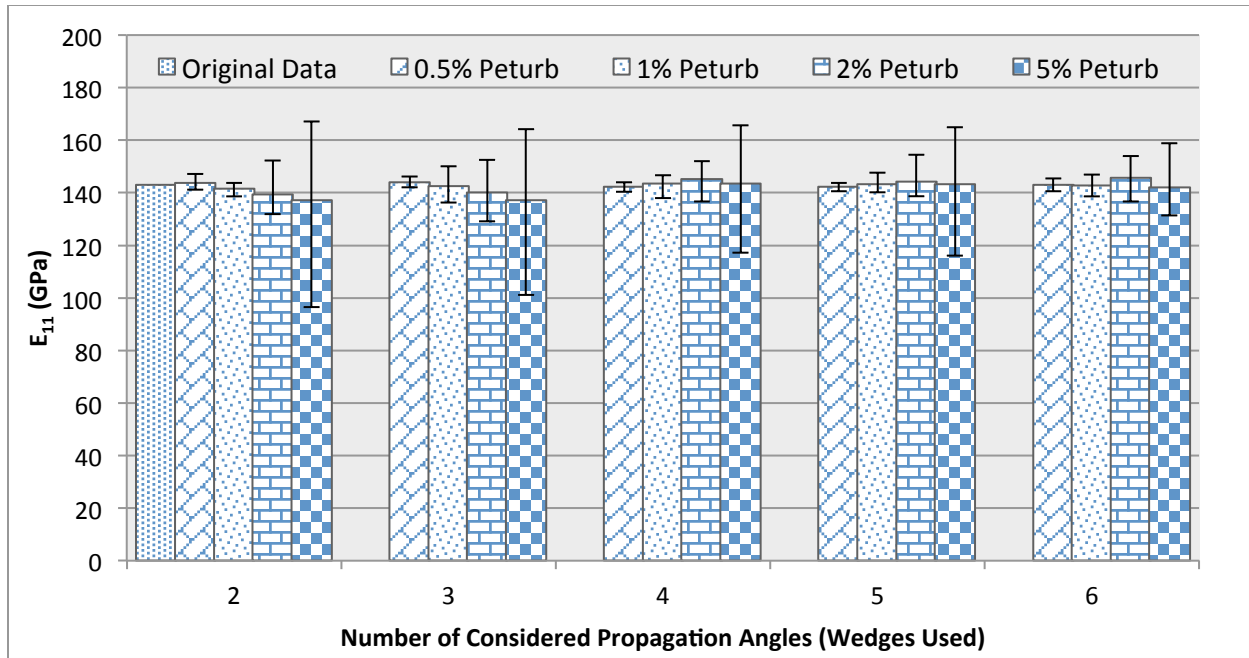
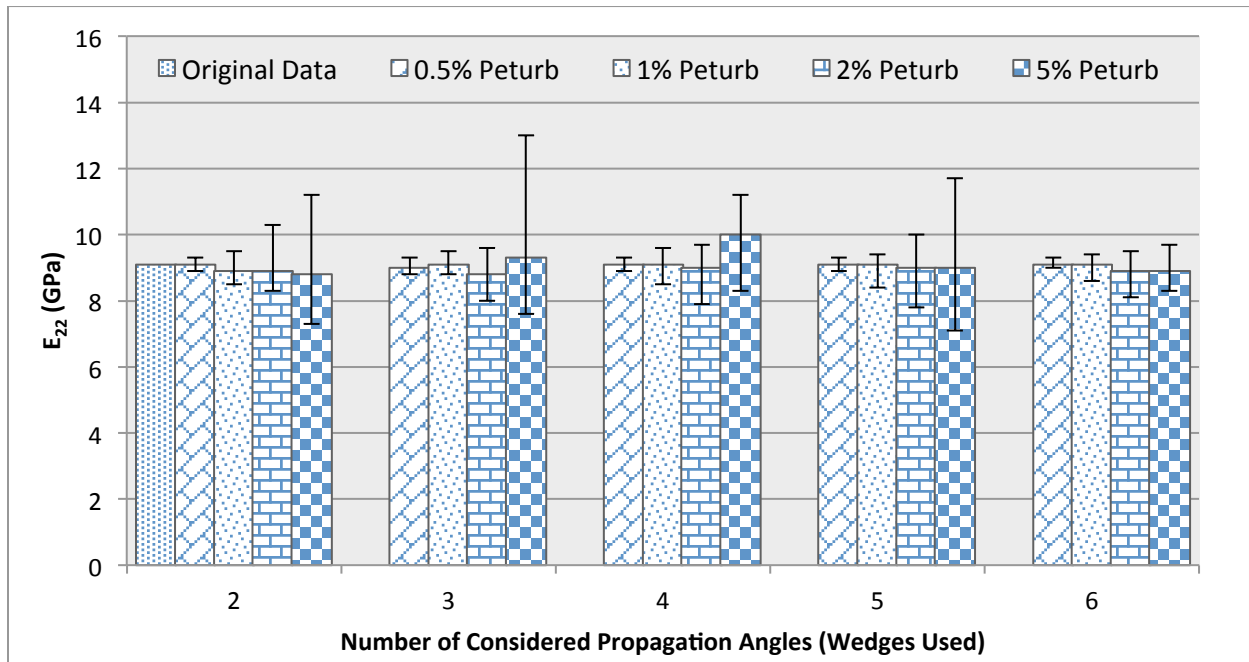**Figure 12: Initial convergence summary of E_{11}**

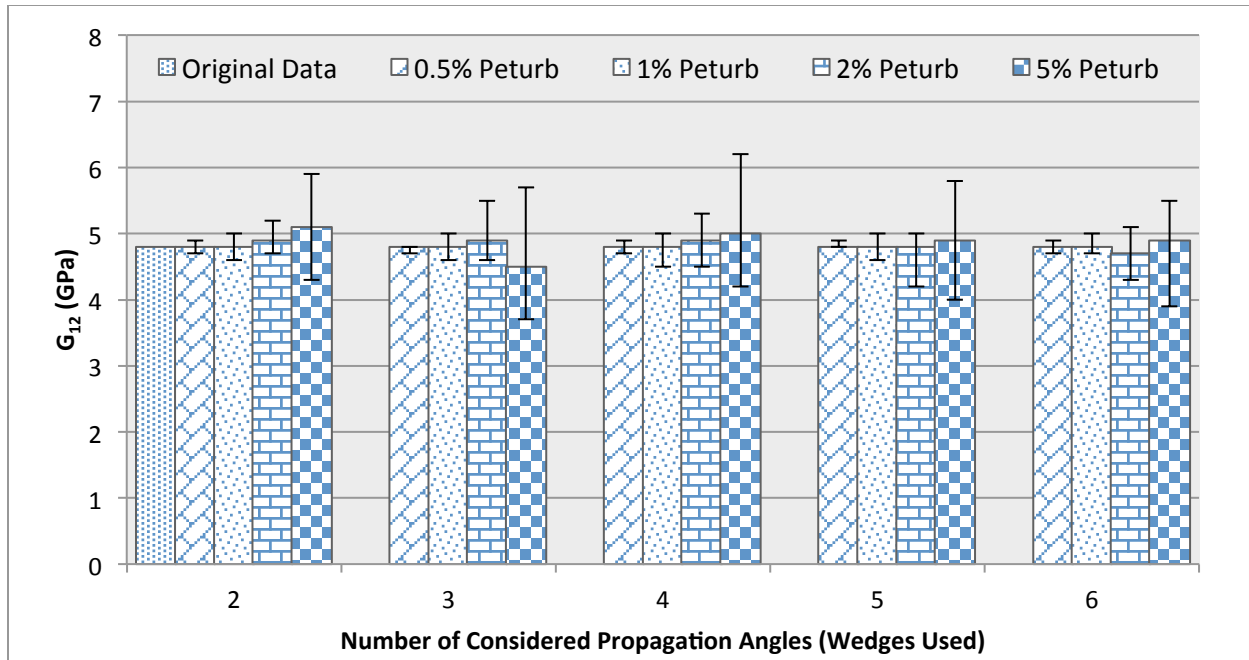**Figure 13: Initial convergence summary of E_{22}**

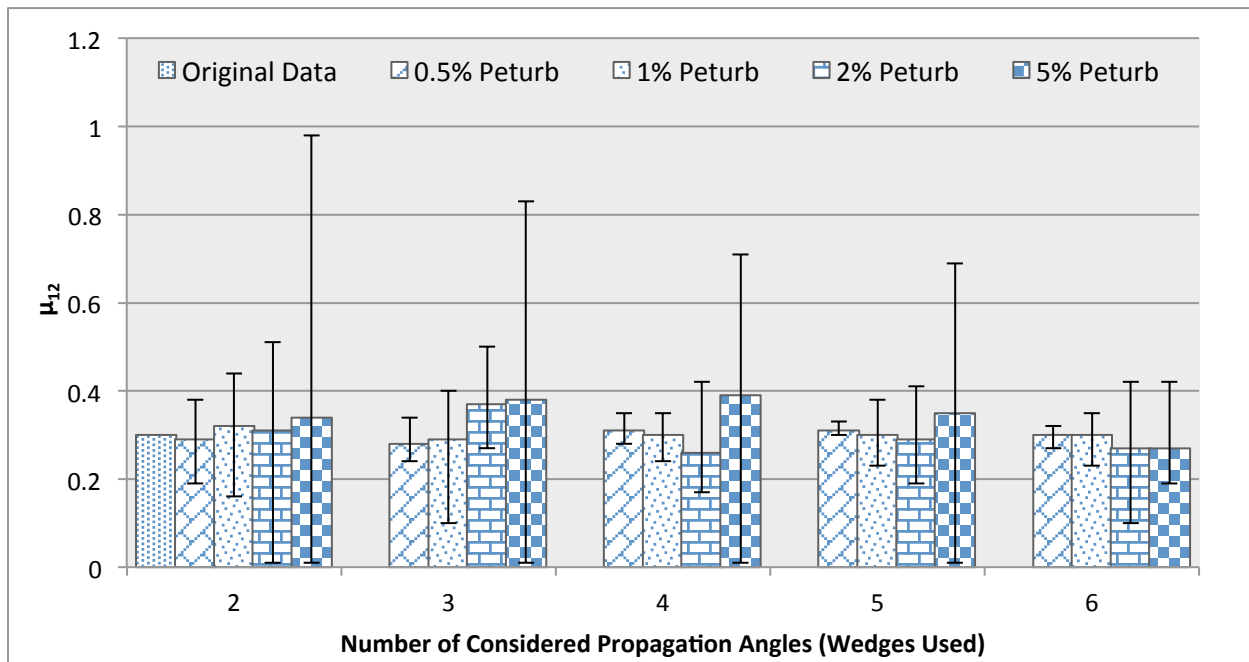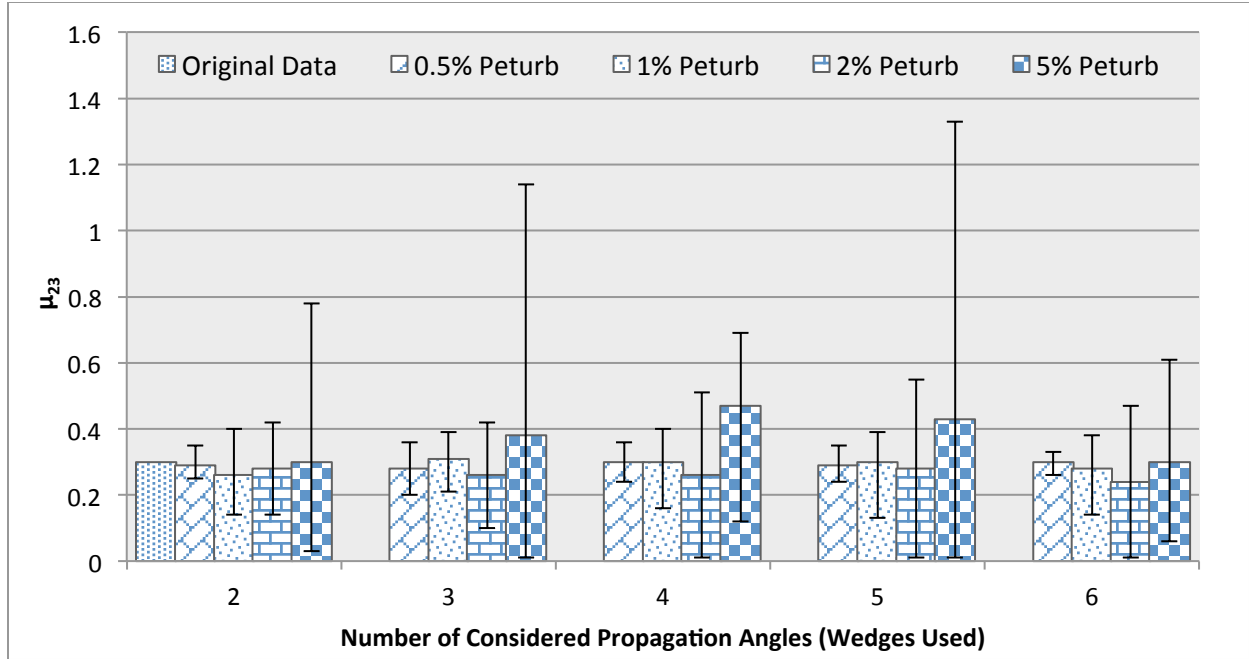**Figure 14: Initial convergence summary of G_{12}**

Figure 15: Initial convergence summary of μ_{12}

Figure 16: Initial convergence summary of μ_{23}

From Figure 12 to Figure 16, it can be seen that unlike for isotropic material, the algorithm converged even when only two different propagation angles were considered. This suggests that a minimum of two propagation angles are required for QL and QT waves propagating in $(x_1 - x_3)$ and $(x_2 - x_3)$ planes for transversely isotropic material. It can also be seen that the errors associated with the data scatter of Poisson's ratios (μ_{12}, μ_{23}) were higher as compared to the tensile and shear stiffness. Therefore, an improvement in the least-squared algorithm for a transversely isotropic material presented above was performed. This improvement consisted of comparing and equating the stiffness matrix constants (c_{33}) calculated using the waves propagating in $(x_1 - x_3)$ and $(x_2 - x_3)$ planes. Also knowing that c_{22} should be equal to c_{33} for a transversely isotropic material; a bisection method was implemented in two steps as shown in Figure 17 within the dotted box. First, the difference between the calculated c_{33} from two different wave propagation planes were minimized. Then, the minimized stiffness constant c_{33} was further compared with c_{22}. During the minimization process the other variables $(c_{11}, c_{13}, c_{23}, c_{55}, c_{44})$ were left to freely change between the upper and lower bounds to satisfy the equality condition.
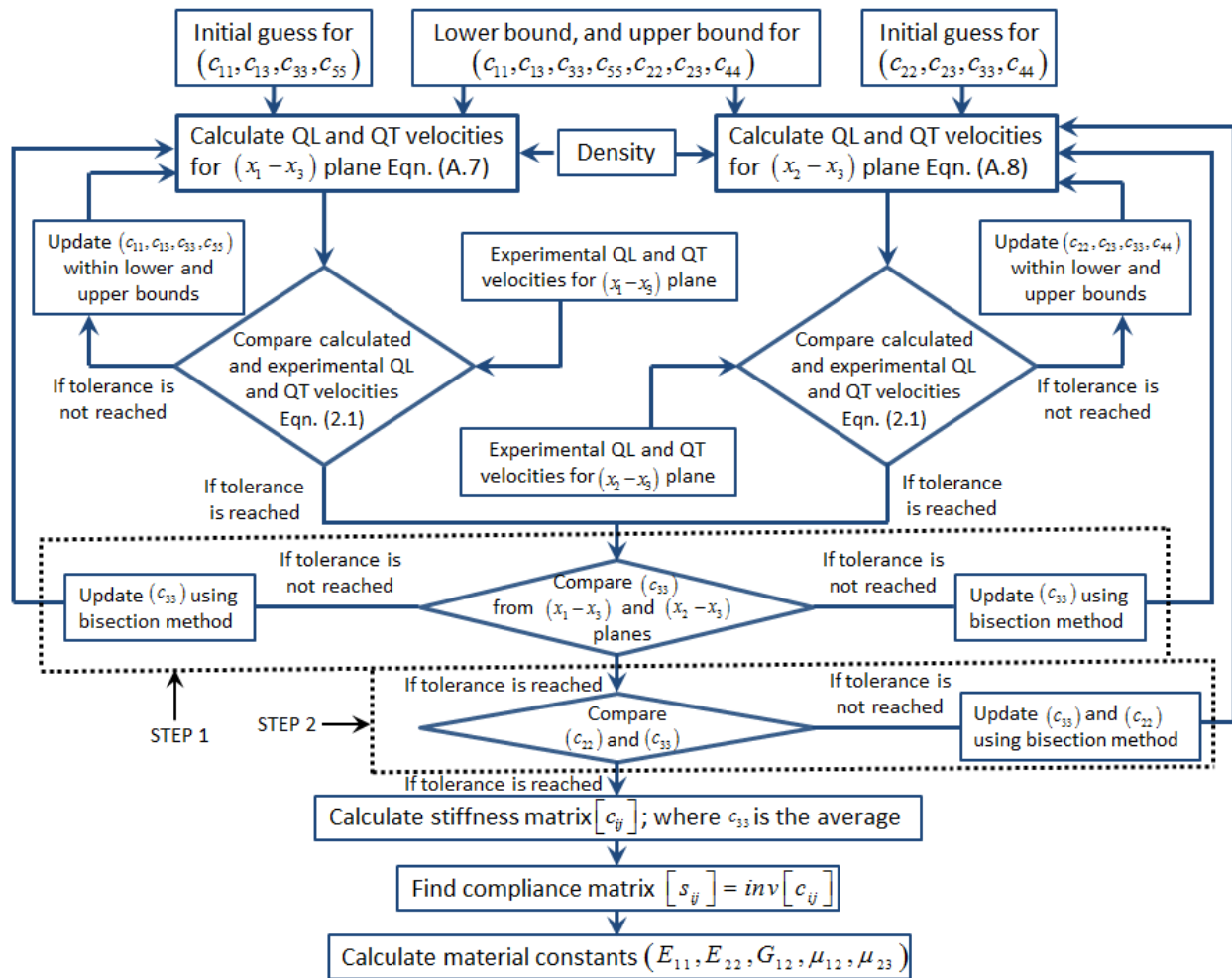
Figure 17: Improved method to find stiffness constant of a transversely isotropic material

This method in turn greatly improved the convergence results especially for E_{22} and μ_{23} as shown in Figure 19 and Figure 22 respectively. The other stiffness constants E_{11} (Figure 18), G_{12} (Figure 20) and μ_{12} (Figure 21) were also improved as compared to the initial algorithm shown in Figure 11.
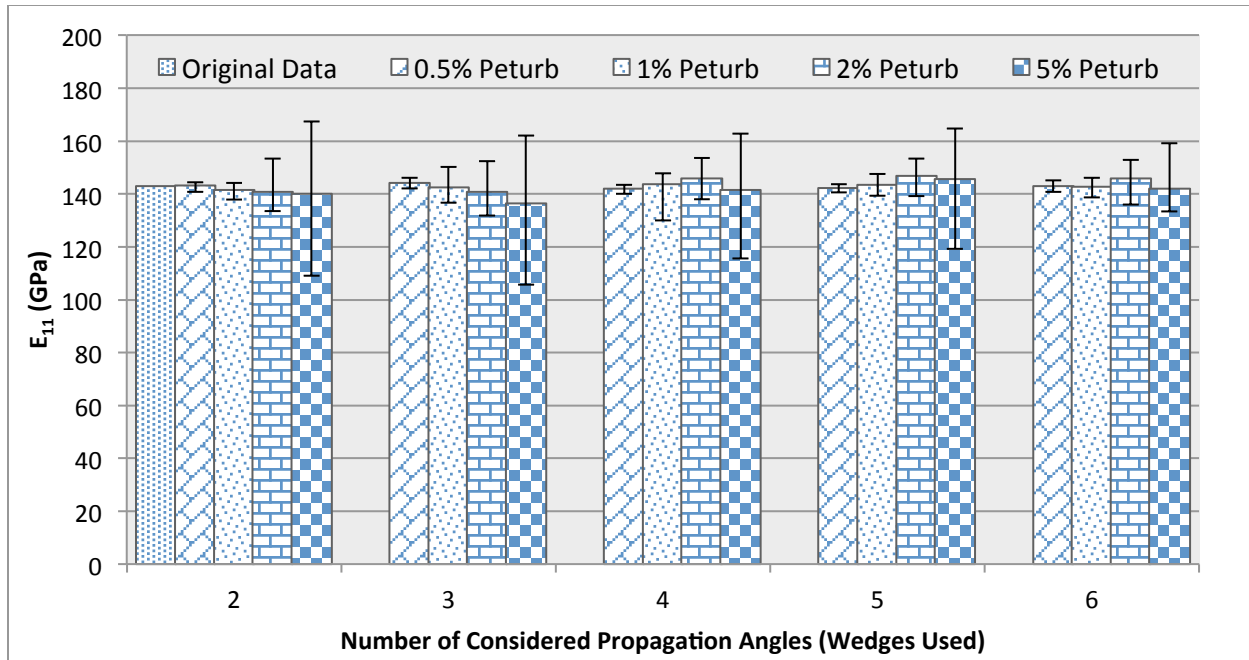
Figure 18: Convergence summary of E_{11} after implementing the improved algorithm
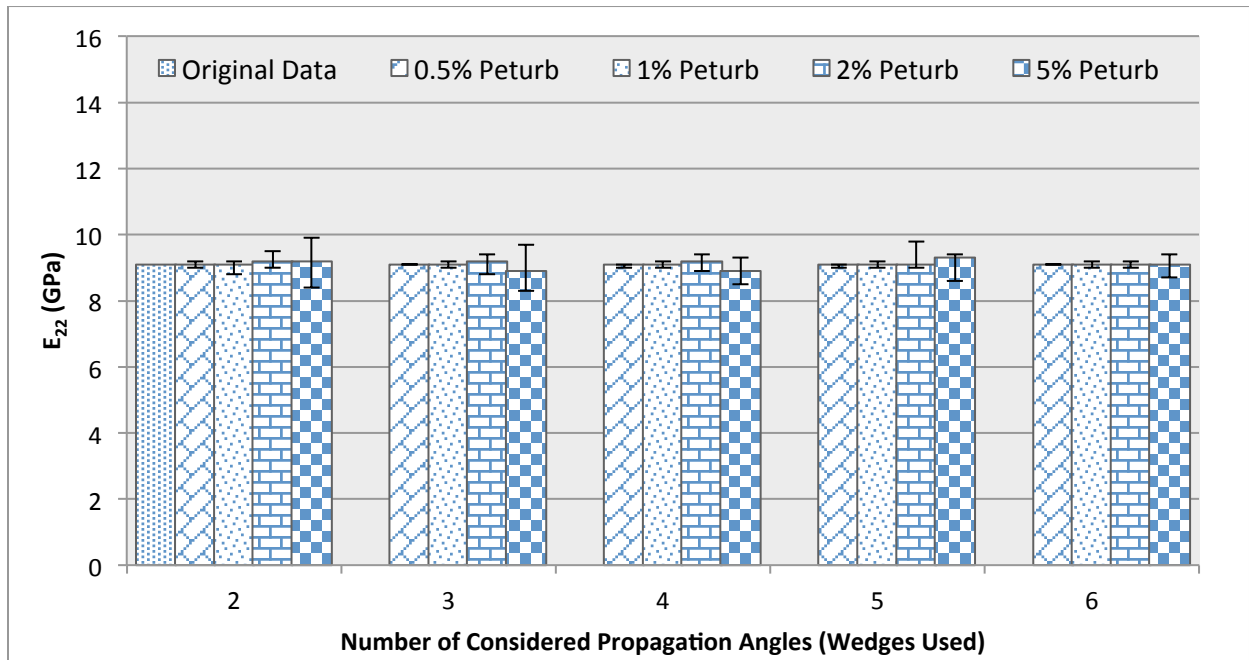
Figure 19: Convergence summary of E_{22} after implementing the improved algorithm
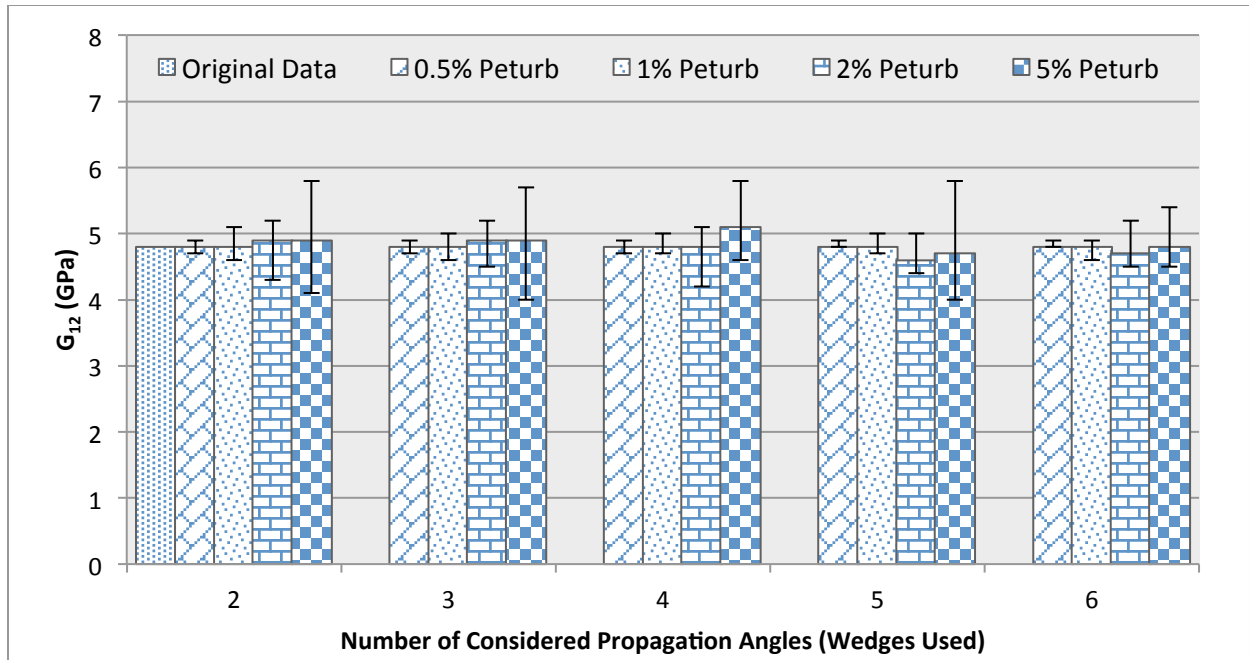
Figure 20: Convergence summary of G_{12} after implementing the improved algorithm
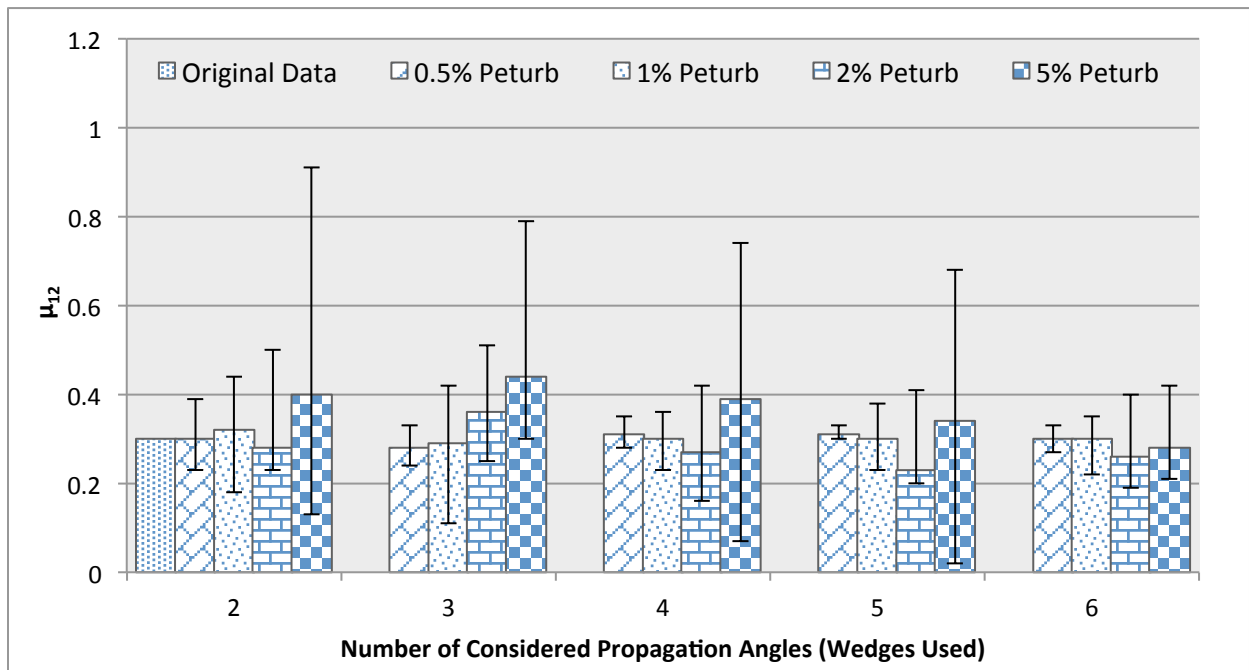
Figure 21: Convergence summary of μ_{12} after implementing the improved algorithm
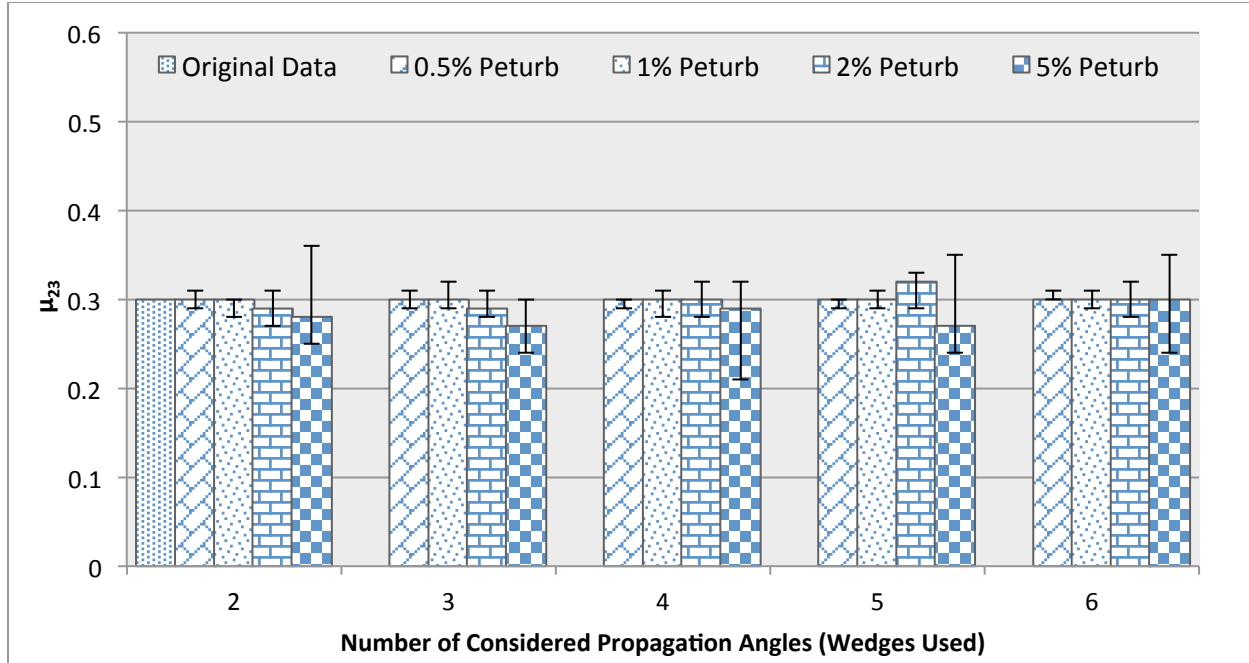
Figure 22: Convergence summary of μ_{23} after implementing the improved algorithm

From Figure 18 to Figure 22 above, it can be seen that a minimum of two sets of propagation angles are required to generate QL and QT waves for the inverse stiffness calculation of transversely isotropic material. Similar to the isotropic case, it was found that changing the initial guesses and the lower/upper bounds had no effects on the final results generated by the improved algorithm.

3 Experimental Results

3.1 Isotropic 7050-T7451 aluminum

Two samples of isotropic aluminum alloy 7050-T7451 aluminum measuring 254 mm by 50.8 mm with thicknesses of 5 mm and 12.7 mm were experimentally tested using the ultrasonic method presented in this paper. Stiffness constants for the 7050-T7451 aluminum sample cut from the same block was experimentally determined previously at Delft University of Technology (TU Delft) [14] using tensile tests following the ASTM E8M-04 standard [15]. The QL and QT waves were generated and acquired using three different angled-wedges as suggested by the sensitivity analysis for isotropic material. The average of three data points were taken for each velocity measurements. The summary of the averaged QL and QT velocities using different wedges for the isotropic 7050-T7451 aluminum is provided in Table 2.

Table 2: Measured QL and QT velocities and propagation angles of 7050-T7451 aluminum specimen

Wave Mode	5 mm Sample		12.7 mm Sample	
	Propagation Angle θ_{13} (Figure A1)	Wave Velocity (m/s)	Propagation Angle θ_{13} (Figure A1)	Wave Velocity (m/s)
QL	37.2°	6247.3	46.9°	6188.9
QL	60.0°	6200.6	60.8°	6188.7
QL	90.0°	6278.2	90°	6235.3

QT	40.2°	3033.0	32.3°	3041.7
QT	42.6°	3060.7	39.8°	3057.6
QT	48.6°	3069.7	46.8°	3076.5

The velocity data in Table 2 was used to inversely calculate the material constants provided in Table 3 using the improved algorithm from Figure 7. In Table 2, the spread of propagation angle is greater for QL as compared to QT because of the Snell's Law. Since the velocity of QL is greater than QT, any small change in the wedge angle created a large change in the through-thickness propagation angle of QL compared to QT.

Table 3: Measured material properties of 7050-T7451 aluminum

	E (GPa)	Poisson's Ratio	G (GPa)	Density (kg/m^3)
Published [16]	71.7	0.33	26.9	2825
Measured using Tensile Test [14]	70.2	0.33	26.4	Not Measured
Measured using ultrasonic techniques presented above				
12.7 mm sample (Using improved algorithm)	71.8	0.34	26.7	2830 (Measured)
5 mm sample (Using improved algorithm)	71.7	0.35	26.6	2830 (Measured)

It can be seen from Table 3 that the results obtained using the non-destructive ultrasonic method presented in this paper were consistent for both thick (12.7 mm) and thin (5 mm) samples with minor discrepancy in the Poisson's ratio. The values for E and G measured using the ultrasonic method were closer to the published data as compared to the values using the mechanical testing. However, the Poisson's ratio was slightly off as compared to both mechanical testing and published value. The discrepancy can be attributed to the experimental error as Poisson's Ratio is most sensitive to random errors compared to E and G. It was also found that the conventional algorithm over predicted both E and Poisson's Ratio as compared to the improved algorithm using the bisection method.

3.2 Transversely Isotropic

In order to validate the ability of the presented non-destructive technique for material characterization of a transversely isotropic material, a blind test was conducted. Collaborators at TU Delft in the Netherlands prepared a series of composite panels, out of which one was shipped to Carleton University, Canada for evaluation. The material properties were then measured at both labs and the results were compared with those obtained from the non-destructive ultrasonic technique presented in this paper.

The sample sent to Carleton University was constructed out of 24 layers of unidirectional carbon-fibre epoxy Cycom 977-2 12 k HTA prepreg. The panels were fabricated in an autoclave following the manufacturer's recommended cure cycle. The cure cycle consisted of: (1) an application of 7 bar gauge autoclave pressure; (2) 1-3°C/min to 177°C; (3) a hold of the temperature and 7 bar gauge pressure at 177°C for 180 minutes; (4) cool down at a rate of 2-5°C/min; (4) a vent of the autoclave pressure when the components reaches 60°C or below. The overall dimension of the sample was approximately 300 mm by 300 mm with an average thickness of 6 mm and the density was measured to be approximately 1700 kg/m^3.

For finding the stiffness constants of the carbon-fiber laminate, experiments were conducted at two different locations. At TU Delft, the stiffness constants of the same material were measured on a Zwick/Roell Hydraulic test frame system Z250 following the ASTM standard D3039-08 [17] for tensile to measure E_{11} and E_{22} and D3518-94 [18] for shear to measure G_{12}. At Carleton University, the carbon-fiber laminate was tested using the ultrasonic technique and tensile tests. For the ultrasonic technique, the QL and QT waves were generated and acquired using three different angled-wedges to improve the convergence as opposed to two as suggested by the sensitivity analysis due to the variation in the sample thickness. The QL and QT waves were measured at two different planes corresponding to $\theta_{12} = 0°$ and 90° angles (Figure A1) with respect to the fibre orientation. An average of three data points were taken for each velocity measurements. Summary of the measured QL and QT velocities at different propagation angles for the transversely isotropic composite laminate is provided in Table 4.

Table 4: Summary of the measured QL and QT velocities of the transversely isotropic specimen

Wave Mode	$\theta_{12} = 0°$ (Figure A1)		$\theta_{12} = 90°$ (Figure A1)	
	Propagation Angle (θ_{13})	Wave Velocity (m/s)	Propagation Angle (θ_{23})	Wave Velocity (m/s)
QL	23.9°	8334.8	45.6°	2801
QL	27°	8179	34°	2755.6
QL	90°	2800.5	90°	2800.5
QT	65.7°	2422.6	43.9°	1637.5
QT	66.4°	2447.6	43.1°	1640.9
QT	70.9°	2501.2	37.7°	1676.5

For laminated composite, the equations provided in Appendix A are based on Representative Volume Elements (RVEs); therefore, it is important that the wavelength of the excited QL and QT waves be sufficiently larger than the micro-structural scale of 7 micro-meters fiber diameter [19], defining the RVEs. This was verified by analysing the frequency content using Fast Fourier Transform (FFT) of the received signal as shown in **Error! Reference source not found.**.

(a) Actuation signal
(b) Received signal
(c) FFT of entire received signal
(d) FFT of the first arriving wave
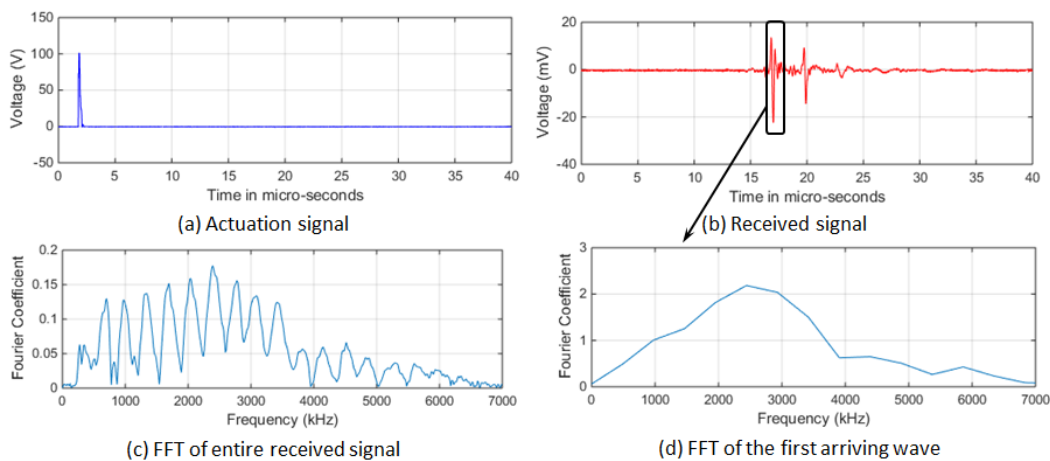
Figure 23: Typical actuation and received signal

Error! Reference source not found. (a) and (b) shows a typical actuation and received signals respectively. **Error! Reference source not found.** (c) shows that the received signal comprises of waves

at different frequencies. Since only the first wave of arrival is considered, the FFT in **Error! Reference source not found.** (d) shows the first arriving wave has the highest frequency content around 2.5 MHz. This was true for other signals that were analyzed, where most of the received signals were concentrated around 2 to 3 MHz frequency band. Wavelengths of the wave excited at 2 to 3 MHz travelling at different velocities are provided in **Error! Reference source not found.**.
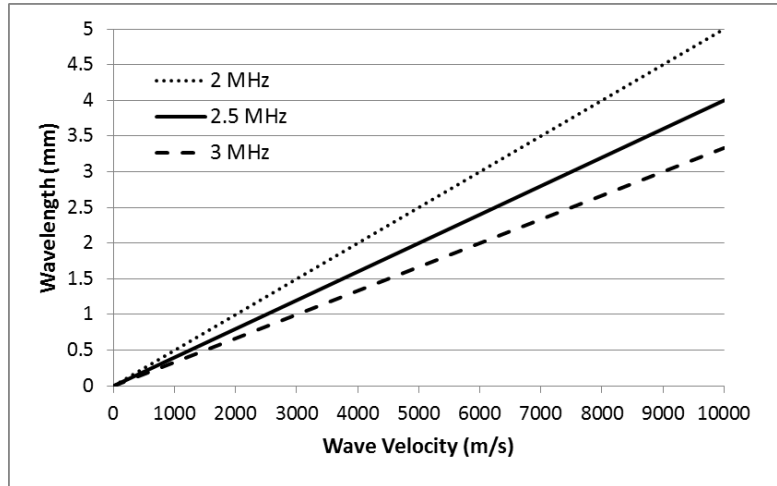
Figure 24: Wavelength at different wave velocities

Using the velocity data from Table 4 and **Error! Reference source not found.**, it can be verified that the smallest wavelength is 0.66 mm corresponding to QT travelling at 1637.5 m/s and 2.5 MHz, which is greater than the fiber diameter and the individual lamina thickness of 0.25 mm.

The velocity data provided in Table 4 was used to inversely calculate the material constants provided in Table 5 using the improved algorithm shown in Figure 17. The initially developed algorithm failed to converge for this type of material characterization. Once the ultrasonic velocity data were obtained, the carbon-fiber laminate was waterjet cut to produce four coupons measuring 25.4 mm by 254 mm each for tensile testing. Two coupons from 0° and 90° fibre orientations were used to measure E_{11} and E_{22} respectively. Coupons from 0° were instrumented with Tee strain gage (CAE-06-125WT-350) to determine the in-plane Poisson's ratio μ_{12}; whereas, MTS-643.12E-24 extensometer was used to measure the induced strains due to applied loads on rest of the coupons for calculating E_{11} and E_{22} stiffness. Transverse Poisson's ratio μ_{23} and shear stiffness G_{12} could not be measured due to limitations in the as constructed carbon-fiber laminate. Results from the tensile tests are presented in Table 5.

Table 5: Measured material properties of transversely isotropic sample

	E_{11} (GPa)	E_{22} (GPa)	G_{12} (GPa)	μ_{12}	μ_{23}
Measured at Carleton using ultrasonic technique and improved algorithm	127.3	11.8	13.4	0.56	0.27
Measured at Carleton using tensile test	119.6	10.9	Not Measured	0.33	Not Measured
Measured at TU Delft using tensile test	125.9	7.7	3.6	0.34	Not Measured

It can be observed from Table 5, that the results obtained using the non-destructive ultrasonic method and the improved algorithm presented in this paper were consistent with the tensile tests conducted on the same laminate with minor discrepancy in the E_{11} and E_{22}. However, the ultrasonic method over-predicted the in-plane Poisson's ratio μ_{12} by 70% and no data were available to compare μ_{23} and G_{12}. However, it is interesting to note that the G_{12} of the carbon fiber filament is around 14 to 18 GPa for fibers similar to the one that was used in this experiment [20]. This discrepancy can be explained due to the tested panel thickness variation of approximately ±0.5 mm corresponding to the percent error in the propagating wave between 1.2 to as high as 7.8 percent. As presented in Figure 18 to Figure 22, even after implementing the improved algorithm, 5% random error in the input velocity data had significant effect on μ_{12} (Figure 21) as compared to the other constants. However, despite the presence of experimental error higher than 5%, the ultrasonic method provided in this paper had an excellent agreement with the tensile tests for E_{11} and E_{22}. The initial algorithm was unable to provide the material properties using the experimental data.

When the results were compared with the tests performed using the same material but following the ASTM standard at TU Delft, the E_{11} stiffness was consistent. However, E_{22} was higher by 53%, G_{12} was higher by 272% and μ_{12} was higher by 65% using the ultrasonic technique. It is to be noted that the coupons were manufactured from the same unidirectional prepreg but with different thicknesses and layups as suggested by the ASTM standard [17] and [18]. This discrepancy can be attributed to the manufacturing variability of laminate samples with different thicknesses and layups corresponding to differences in the overall material stiffness properties.

4 Conclusion

An *in-situ* method for measuring the material properties with access to only one side of the specimen is presented. The technique uses generating and receiving quasi-longitudinal and quasi-transverse waves at different through-thickness angles using angled-wedges. First, the analytical equations were derived for an isotropic and transversely isotropic material. Then, an inverse method based on the non-linear least square technique was used to calculate the stiffness constants using the ultrasonic wave velocities. Sensitivity analysis was performed by randomly perturbing the velocity data and observing its effect on the calculated stiffness constants. An improved algorithm was proposed and tested to reduce the effects of random experimental errors. Based on the sensitivity analysis, a minimum number of angled-wedges required to inversely calculate the stiffness constants were determined. It was found that a minimum of three and two angled-wedges (corresponding to number of different propagation angles) were needed to inversely calculate the stiffness constants for an isotropic and a transversely isotropic material respectively.

The method was then experimentally verified on an isotropic aluminum alloy 7050-T7451 aluminum with two different thicknesses and a transversely isotropic composite laminate fabricated using 24 plies of carbon-fibre epoxy Cycom 977-2 12 k HTA unidirectional prepregs. As expected for an isotropic aluminum, at lower wedge angles, below the first critical angle, quasi-longitudinal wave was more distinct. Whereas, for the wave travelling between the first and the second critical angle quasi-transverse wave was more prominent. The results were consistent for both thick (12.7 mm) and thin (5 mm) isotropic 7050-T7451 aluminum samples with minor discrepancy in the Poisson's ratio. The values for E and G measured using the ultrasonic method were closer to the published data as compared to the values using the mechanical testing. As for the transversely isotropic sample, it was found that E_{11} and E_{22}

agreed well with the presented ultrasonic method and the tensile test, despite having in excess of 5% experimental error due to the sample thickness variation. However, for the in-plane Poisson's ratio μ_{12}, the discrepancy was approximately 70% between the ultrasonic method and the tensile experiment. This is because μ_{12} is most sensitive to the random error as compared to other stiffness constants found by the sensitivity analysis. No data were available for comparing the transverse Poisson's ratio μ_{23} and shear stiffness G_{12}. When the results were compared with the tests performed following the ASTM standard at TU Delft, the E_{11} stiffness was consistent. However, E_{22} was higher by 53%, G_{12} was higher by 272% and μ_{12} was higher by 65% using the ultrasonic technique due to the manufacturing variability of laminate samples with different thicknesses and layups.

Therefore, it can be concluded that the method presented in this paper is more accurate for the isotropic material as compared to the transversely isotropic material. For transversely isotropic material the ultrasonic method presented here works well if the experimental errors can be reduced to less than 1%. Also the ultrasonic method was able to better predict the material properties E_{11} and E_{22} of the as manufactured sample.

## Acknowledgements

References

1. Ostiguy, P. C., Quaegebeur, N., Mulligan, K. R., Masson, P., and Elkoun, S., "In situ mechanical characterization of isotropic structures using guided wave propagation," *Smart Materials and Structures*, Vol. 21, No. 4, 2012, doi:10.1088/0964-1726/21/6/065010.
2. Papadakis, E. P., "Ultrasonic wave measurements of elastic moduli E, G, μ for product development and design calculations," *American Society for Testing and Materials*, Vol. 26, No. 3, 1998, p 240-246, doi:10.1520/JTE11997J
3. France, E. E., Meza, J. M., and Buiochi, F., "Measurement of elastic properties of materials by the ultrasound through-transmission technique," *DYNA*, Vol. 168, No. 168, 2011, p 59-64.
4. ASTM E494-102010: Standard practice for measuring ultrasonic velocity in materials, ASTM International, West Conshohocken, PA, 2010, www.astm.org
5. Van Buskirk, W. C., Cowin, S. C., and Carter, R., "A theory of acoustic measurement of the elastic constants of a general anisotropic solid," *Journal of Materials Science*, Vol. 21, No. 8, 1986, p 2759-2762, doi:10.1007/BF00551484.
6. Stijnman, P.W.A., "Determination of the Elastic Constants of Some Composites by using Ultrasonic Velocity Measurements," *Composites*, Vol. 26, No. 1995, p 597-604, doi:10.1016/0010-4361(95)92624-L.
7. Kohlhauser, C., Hellmich, C., "Determination of Poisson's ratio in isotropic, transversely isotropic, and orthotropic materials by means of combined ultrasonic-mechanical testing of normal stiffnesses: Application to metals and wood," European Journal of Mechanics A/Solids, Vol. 33, 2012, p 82-98, doi:10.1016/j.euromechsol.2011.11.009.

8. J.D.N. Cheeke, *Fundamentals and applications of ultrasonic waves*, 2nd ed., CRC Press, 2002, p. 101-123.

9. Balasubramaniam, K., and Rao, N.S., "Inversion of composite material elastic constants from ultrasonic bulk wave phase velocity data using genetic algorithms," *Composite Part B: Engineering,* Vol. 29, No. 2, 1998, p 171–180, doi:10.1016/S1359-8368(97)00007-3.

10. Chu, Y.C., and Rokhlin, S.I., "A method for determination of elastic constants of a unidirectional lamina from ultrasonic bulk velocity measurements on [0/90] cross-ply composites," *Journal of Acoustical Society of America*, Vol. 96, 1994, p 342-352, doi:10.1121/1.410484.

11. Liu, G.R., Han, X., Lam, K.Y., "A combined genetic algorithm and nonlinear least squares method for material characterization using elastic waves," *Computer Methods in Applied Mechanics and Engineering*, Vol. 191, No. 17-18, 2002, p 1909-1921, doi:10.1016/S0045-7825(01)00359-0.

12. Aluminum 2024-T6, Aerospace Specification Metals (ASM) Inc, http://asm.matweb.com/search/SpecificMaterial.asp?bassnum=MA2024t6, (Accessed Feb 1, 2016).

13. Pant, S., Laliberte, J., Martinez, M., Rocha, B., Ancrum, D., "Effects of composite lamina properties on fundamental Lamb wave mode dispersion characteristics," *Journal of Composite Structures*, Vol. 124, 2015, p 236-252, doi:10.1016/j.compstruct.2015.01.017.

14. Lotz, T., "Development of a consistent experimental method to study residual stress effects on fatigue crack growth," Master's Thesis, Delft University of Technology, 2014.

15. ASTM E8M-04: Standard test method of tension testing of metallic materials at room temperature, ASTM International, West Conshohocken, PA, 2004, www.astm.org.

16. MIL-HDBD-5H - Table 3.7.4.0(b1): Metallic materials and elements for aerospace vehicle structures design mechanical and physical properties of 7050 aluminum alloy plate, 2001.

17. ASTM D3039/D3039M-08: Standard test method for tensile properties of polymer matrix composite materials, ASTM International, West Conshohocken, PA, 2008, www.astm.org.

18. ASTM D3518/D3518M-94: Standard test method for in-plane shear response of polymer matrix composite materials by tensile test of a ±45° laminate (Reapproved 2007), ASTM International, West Conshohocken, PA, 2007, www.astm.org.

19. Toho Tenax G30-500 12k HTA-7C NSO1 Continuous Filament Carbon Fiber, http://www.matweb.com/search/datasheet.aspx?matguid=fb15fd5e0cae4ed2bb5df24164213827&ckck=1, (Accessed Feb 4, 2016).

20. Chung, D. D. L., Carbon Fiber Composites, 1st ed., Butterworth-Heinemann, 1994, p. 72.

21. Degtyar, A.D. and Rokhlin, S.I., "Comparison of Elastic Constant Determination in Anisotropic Materials from Ultrasound Group and Phase Velocity Data," *Journal of Acoustical Society of America*, Vol. 102, 1997, p 3458, doi:10.1121/1.419588.

Appendix A: Ultrasonic Wave Equations

For the relationship between the ultrasonic wave velocity and material properties, consider a plate with thickness of *2h* with the associated co-ordinates shown in Figure A1.
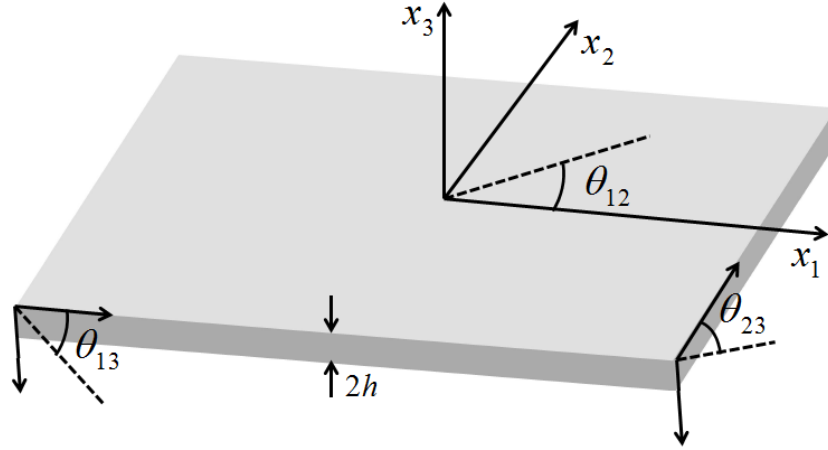
Figure A1: Transversely isotropic plate with the coordinate system

The general equation of motion without considering the body forces for the plate can be written as:

$$c_{ijkl} \frac{\partial^2 u_k}{\partial x_j \partial x_l} = \rho \frac{\partial^2 u_i}{\partial t^2} \tag{A.1}$$

Where, c_{ijkl} is the stiffness constant, ρ is the density, x_i is the direction, u_i is the displacement, and t is time.

The displacement u_i is assumed to be a simple harmonic of the form:

$$u_i = U_i e^{i(kn_j x_j - \omega t)} \tag{A.2}$$

Where, U_i is the displacement amplitude, k is the wave number, n_j is the unit vector, and ω is the circular frequency.

Taking the partial derivative of the displacement u_i with respect to direction x_i and time t and substituting the partial derivatives back into the equilibrium equation Eqn. (A.1) gives the well-known Christoffel equation in a matrix form as:

$$\begin{bmatrix} \Lambda_{11} - \rho c_p^2 & \Lambda_{12} & \Lambda_{13} \\ \Lambda_{12} & \Lambda_{22} - \rho c_p^2 & \Lambda_{23} \\ \Lambda_{13} & \Lambda_{23} & \Lambda_{33} - \rho c_p^2 \end{bmatrix} \begin{Bmatrix} U_1 \\ U_2 \\ U_3 \end{Bmatrix} = 0 \tag{A.3}$$

Where, c_p is the phase velocity and the elements of Λ_{il} are given in terms of propagation directions by:

$$\Lambda_{11} = c_{11}n_1^2 + c_{66}n_2^2 + c_{55}n_3^2$$
$$\Lambda_{12} = (c_{12} + c_{66})n_1 n_2$$
$$\Lambda_{13} = (c_{13} + c_{55})n_1 n_3$$
$$\Lambda_{22} = c_{66}n_1^2 + c_{22}n_2^2 + c_{44}n_3^2 \tag{A.4}$$
$$\Lambda_{23} = (c_{23} + c_{44})n_2 n_3$$
$$\Lambda_{33} = c_{55}n_1^2 + c_{44}n_2^2 + c_{33}n_3^2$$

Equation (A.3) is the mathematical representation of an eigenvalue problem of phase velocity c_p^2, which defines three homogeneous linear equations of displacement amplitudes (U_1, U_2, U_3). The three solutions represent a quasi-longitudinal, a quasi-transverse-vertical, and a transverse-horizontal waves propagating within the material along different directions. The solution to Eqn. (A.3) and hence the phase velocities c_p^2 can be found by setting the determinant to be zero. Eqn. (A.3) can be further simplified by considering the waves propagating in the through thickness direction along two-dimensional planes of symmetry (principal planes). For isotropic material the wave propagating in the principal plane $(x_1 - x_3)$ along the refracted angle θ_{13} measured with respect to the x_1 axis is considered (Figure A1). For transversely isotropic material additional waves propagating in the principal plane $(x_2 - x_3)$ along the refracted angle θ_{23} measured with respect to the x_2 axis must be considered (Figure A1).

The unit vector n_i for the wave propagating in $(x_1 - x_3)$ plane can be expressed as:

$$n_i = (n_1, n_2, n_3) = (\cos\theta_{13}, 0, \sin\theta_{13}) \tag{A.5}$$

Therefore, determinant of Eqn. (A.3) can be reduced to:

$$\begin{vmatrix} \Lambda_{11} - \rho c_p^2 & 0 & \Lambda_{13} \\ 0 & \Lambda_{22} - \rho c_p^2 & 0 \\ \Lambda_{13} & 0 & \Lambda_{33} - \rho c_p^2 \end{vmatrix} = 0 \tag{A.6}$$

As mentioned earlier, Eqn. (A.6) can be decomposed into three waves, which are: transverse-horizontal (T), quasi-longitudinal (QL) and quasi-transverse-vertical (QT) waves and are given by [21]:

$$\rho c_{p(T)}^2 = \Lambda_{22}$$
$$\rho c_{p(QL)}^2 = \left(\frac{\Lambda_{11} + \Lambda_{33}}{2}\right) + \frac{\sqrt{(\Lambda_{11} - \Lambda_{33})^2 + 4\Lambda_{13}^2}}{2} \tag{A.7}$$
$$\rho c_{p(QT)}^2 = \left(\frac{\Lambda_{11} + \Lambda_{33}}{2}\right) - \frac{\sqrt{(\Lambda_{11} - \Lambda_{33})^2 + 4\Lambda_{13}^2}}{2}$$

Therefore, knowing the phase velocity, which is also equal to the group velocity for the wave propagating in the principal direction, it is possible to inversely calculate the stiffness matrix using Eqn. (A.7) and hence, find the material properties of an isotropic solid. Similar to $(x_1 - x_3)$ plane, three waves: transverse-horizontal (*T*), quasi-longitudinal (*QL*) and quasi-transverse-vertical (*QT*) waves exist for the $(x_2 - x_3)$ plane as well and are given by [21]:

$$\rho c^2_{p(T)} = \Lambda_{11}$$

$$\rho c^2_{p(QL)} = \left(\frac{\Lambda_{22} + \Lambda_{33}}{2} \right) + \frac{\sqrt{(\Lambda_{22} - \Lambda_{33})^2 + 4\Lambda_{23}^2}}{2}$$

$$\rho c^2_{p(QT)} = \left(\frac{\Lambda_{22} + \Lambda_{33}}{2} \right) - \frac{\sqrt{(\Lambda_{22} - \Lambda_{33})^2 + 4\Lambda_{23}^2}}{2}$$

(A.8)

Using the quasi-longitudinal or quasi-transverse-vertical waves propagating in the $(x_1 - x_3)$ plane, four linear elastic constants $(c_{11}, c_{13}, c_{33}, c_{55})$ can be found. Similarly, by considering the wave propagating in the $(x_2 - x_3)$ plane, four more elastic constants $(c_{22}, c_{23}, c_{33}, c_{44})$ can be found for a transversely isotropic material.

Nomenclature

Symbols	Description	Units
Λ_{il}	Christoffel matrix components	
ω	Circular wave frequency	Rad/s
ρ	Density	kg/m^3
x_i	Direction	
n_j	Directional unit vector	
u_i	Displacement	m
U_i	Displacement amplitude	m
i	Imaginary number	
E	Longitudinal elastic constant	N/m^2
inv	Matrix inverse	
c_p	Phase velocity	m/s
h	Plate half-thickness	m
μ	Poisson's ratio	
QL	Quasi-longitudinal waves	
G	Shear elastic constant	N/m^2
c_{ijkl}	Stiffness elastic constants	N/m^2
SW	Surface waves	
t	Time	s
Φ	Vertical wave incident angle (wedge angle)	$Degrees$
θ_{ij}	Wave propagation direction	$Degrees$
k	Wavenumber	s^{-1}
QT	Quasi-transverse waves	
T	Transverse-horizontal waves	